Trans-nodal migration of resident dendritic cells into medullary interfollicular regions initiates immunity to influenza vaccine

Trans-nodal migration of resident dendritic cells into medullary interfollicular regions initiates immunity to influenza vaccine

Matthew C. Woodruff,[1,4] Balthasar A. Heesters,[4,5] Caroline N. Herndon,[4] Joanna R. Groom,[6] Paul G. Thomas,[7] Andrew D. Luster,[1,8] Shannon J. Turley,[1,3,9] and Michael C. Carroll[1,2,4]

[1]Graduate Program in Immunology, [2]Department of Pediatrics, and [3]Department of Microbiology and Immunobiology, Harvard Medical School, Boston, MA 02115
[4]The Program in Cellular and Molecular Medicine, Children's Hospital Boston, Boston, MA 02115
[5]Department of Medical Microbiology, University Medical Center Utrecht, 3584 CX Utrecht, Netherlands
[6]Department of Medical Biology, The Walter and Eliza Hall Institute of Medical Research, University of Melbourne, Parkville, Victoria 3052, Australia
[7]Department of Immunology, St. Jude Children's Research Hospital, Memphis, TN 38105
[8]Division of Rheumatology, Allergy, and Immunology, Center for Immunology and Inflammatory Diseases, Massachusetts General Hospital, Harvard Medical School, Charlestown, MA 02129
[9]Department of Cancer Immunology and AIDS, Dana-Farber Cancer Institute, Boston, MA 02215

Dendritic cells (DCs) are well established as potent antigen-presenting cells critical to adaptive immunity. In vaccination approaches, appropriately stimulating lymph node–resident DCs (LNDCs) is highly relevant to effective immunization. Although LNDCs have been implicated in immune response, their ability to directly drive effective immunity to lymph-borne antigen remains unclear. Using an inactive influenza vaccine model and whole node imaging approaches, we observed surprising responsiveness of LNDC populations to vaccine arrival resulting in a transnodal repositioning into specific antigen collection sites within minutes after immunization. Once there, LNDCs acquired viral antigen and initiated activation of viral specific CD4$^+$ T cells, resulting in germinal center formation and B cell memory in the absence of skin migratory DCs. Together, these results demonstrate an unexpected stimulatory role for LNDCs where they are capable of rapidly locating viral antigen, driving early activation of T cell populations, and independently establishing functional immune response.

CORRESPONDENCE
Michael C. Carroll:
michael.carroll@childrens.harvard.edu

Abbreviations used: ALN, auricular LN; cDC, conventional DC; cIFR, cortical IFR; IFR, interfollicular region; LNDC, LN-resident DC; mDC, migratory DC; mIFR, medullary IFR; MP-IVM, multiphoton intravital microscopy; MPM, multiphoton microscopy; PLN, popliteal LN; vG, van Gogh.

Since early descriptions of DCs as primary stimulators of adaptive immunity (Steinman, 1991), their role in establishing and regulating immune responses has been central to diverse immunological fields such as transplantation (Larsen et al., 1990; Hill et al., 2011), autoimmunity (Llanos et al., 2011), infectious disease (Poudrier et al., 2012), and vaccinology (Arnason and Avigan, 2012). As critical mediators of antigen presentation, significant effort has been spent describing activation of conventional DCs (cDCs) in peripheral tissue (Moodycliffe et al., 1994; Austyn, 1996; Rescigno et al., 1997) and characterization of their subsequent migration to secondary lymphoid organs (Itano et al., 2003; Randolph et al., 2005; Alvarez et al., 2008; Braun et al., 2011; Tal et al., 2011). Once in peripheral LNs, migratory DC (mDC) populations from the injection site present antigen to cognate T and B cells and stimulate adaptive immunity (Qi et al., 2006).

The activation and maturation of mDCs is thought to follow a three-stage process. First, immature DCs encounter antigen in the periphery, leading to up-regulation of MHC class II and co-stimulatory molecules with a concomitant reduction in phagocytic capacity (Rescigno et al., 1997). Second, antigen-loaded DCs acquire migratory capacity through the expression of matrix metalloproteases (Yen et al., 2008), migratory adhesion molecules (Acton et al., 2012), and rapid actin treadmilling to enter and migrate

The Rockefeller University Press $30.00
J. Exp. Med. 2014 Vol. 211 No. 8 1611-1621
www.jem.org/cgi/doi/10.1084/jem.20132327

The Journal of Experimental Medicine

along lymphatic vessels (Lämmermann et al., 2008). Finally, LN-bound mDCs cross the subcapsular sinus floor into the paracortical region and interact with cognate T cells and LN-resident DCs (LNDCs) within the draining LN (Allan et al., 2006; Braun et al., 2011) to establish protective downstream immunity.

After antigen capture in peripheral tissues, the activation and migration of mDCs into draining LNs is delayed for up to 18–24 h to allow for transcriptional and translational modification and a crawling migration sometimes representing distances of thousands of cell body lengths of the mDC. In the case of vaccination, however, arrival of injected antigen is rapid, with detectable antigen arriving in the draining LN via the afferent lymphatics within minutes (Roozendaal et al., 2009; Gonzalez et al., 2010). This timing discrepancy between antigen arrival in the LN and the migration of DCs from the periphery leaves open a potential window whereby targeting a vaccine to a nondegradative, immunostimulatory compartment within the LN could have important humoral immune ramifications.

Several studies have focused on the drainage of lymph-borne antigen from the afferent lymph into the subcapsular sinus of the draining LN (Szakal et al., 1983; Carrasco and Batista, 2007; Junt et al., 2007; Phan et al., 2007; Roozendaal et al., 2009; Gonzalez et al., 2010). A current view is that subcapsular sinus macrophages rapidly capture antigen from the lymph and participate in its active transport to the B cell follicle. Less well described is the downstream filtration of the lymph within the medulla by medullary sinus-lining macrophages (Gray and Cyster, 2012) and LNDCs (Gonzalez et al., 2010). Historically, DCs residing in the LN (LNDCs) have been described as relatively sessile at steady-state, (Steinman et al., 1997; Lindquist et al., 2004) and insufficient to drive effective immunity after direct antigen acquisition (Itano et al., 2003; Allenspach et al., 2008). However, the recent observation of direct viral capture in the medulla by the LNDC population suggested they may have a more active role in the establishment of downstream immune response in the case of influenza vaccination (Gonzalez et al., 2010).

To extend our understanding of the role of LNDCs in establishing immune response to influenza vaccination, resident DCs were characterized at a whole-LN level. Unexpectedly, a major trans-nodal repositioning of LNDCs from the T cell cortex to the afferent medulla was observed within minutes of viral antigen arrival from the afferent lymphatics, areas recently shown to be important in vaccine efficacy (Liu et al., 2014). This migration leads to rapid viral acquisition by LNDCs and stimulation of viral-specific naive $CD4^+$ T cells. Furthermore, total elimination of skin mDCs had a negligible effect on the generation of a protective humoral response in mice vaccinated with UV-inactive virus. Collectively, the results suggest a model in which LNDCs are fully competent in establishing robust, long-term viral immunity, even in the absence of mDCs from the injection site.

RESULTS

Activation of LNDCs after influenza vaccination

To characterize LNDC response after vaccination, CD11c-eYFP C57BL/6 mice (Lindquist et al., 2004; Hickman et al., 2008; Sung et al., 2012; Kastenmüller et al., 2013) were immunized s.c. in the footpad with UV-inactivated influenza A virus strain PR8 (UV-PR8). DCs were tracked by multiphoton intravital microscopy (MP-IVM) of the popliteal LN (PLN) by surgically exposing the node in live, anesthetized mice (Gonzalez et al., 2010). Continuous imaging for 40 min after UV-PR8 vaccination revealed an influx of LNDCs proximal to the collagen capsule (<150 µm; Fig. 1 a and Video 1). Quantitation of cellular trafficking over this period identified a three- to fourfold increase in the number of YFP^+ DCs within this region (3.23 ± 0.24; $P < 0.001$), suggesting a rapid repositioning to the periphery of the PLN.

In addition to increased cell number within the LN periphery, LNDCs exhibited extensive morphological changes over the 40-min imaging period (Fig. 1 a, inset). Measured in bulk, DCs within these regions increased in surface area by almost 50% after vaccination and experienced a concomitant increase in volume and decrease in spherical index, a measure of the spherical nature of an object (Fig. 1 c and not depicted). Importantly, the fluorescence intensity of individual DCs did not change over this time period, indicating that the observed phenotypic changes were not caused by changes in YFP expression. Together, these data suggest an unexpected accumulation and activation of resident DCs in the PLN periphery immediately after vaccination.

Repositioning of LNDCs to the medulla

To address the origin of the accumulating DCs, in vivo cellular tracking was applied to the live imaging model. By tracking individual DCs, it was observed that rather than infiltrating from an outside source, the cells originated from the interior of the PLN (>150 µm from the collagen capsule), which is beyond the imaging depth threshold for our imaging system (Fig. 1 b and Video 1). Pretreatment of mice with CD62L blocking antibody or local administration of Pertussis toxin, two approaches which limit influx of leukocytes from the vasculature or lymphatics, had negligible effects on DC accumulation (not depicted). These results provide additional evidence that the activated DCs originated within the PLN before vaccination and confirmed their identity as LNDCs.

To assess the overall movement of LNDCs after vaccination, 50-µm serial cryosections of PLNs were imaged by multiphoton microscopy (MPM) and serially reconstructed for analysis of whole PLNs. Similar approaches were reported by Grigorova et al. (2010) using confocal microscopy for partial PLN imaging. By in vivo labeling medullary macrophages through preinjection of an α-F4/80 mAb into the footpad of CD11c-eYFP reporter mice, the medulla could be outlined and shown to include relatively sparse populations of LNDCs in resting naive LNs (Fig. 1 d). In agreement with the live imaging data, injection of UV-PR8 into the footpad of CD11c-eYFP mice stimulated a visible shift of the LNDC population into the medullary compartment by 60 min after vaccination (Fig. 1 d). Flow cytometric analysis of single cell suspensions of PLN indicated no appreciable increase of LNDCs at these time points. This global repositioning of the LNDCs can be

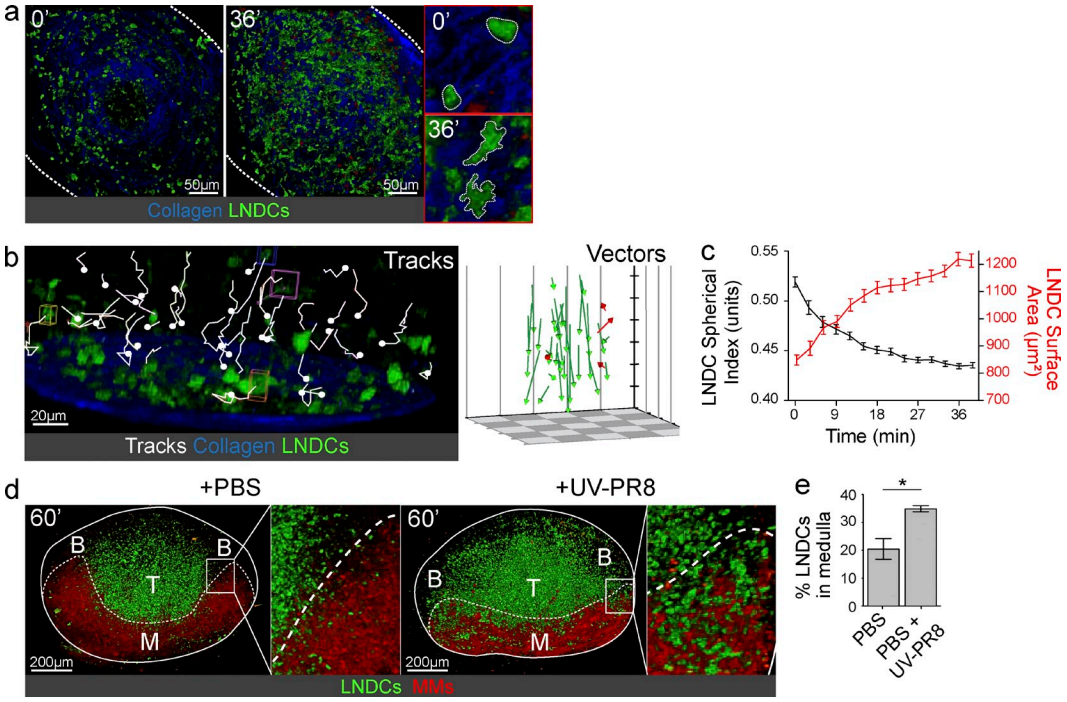

Figure 1. LNDCs migrate to the medulla after influenza vaccination. (a) MP-IVM of DC arrival in the PLN periphery after UV-PR8 vaccination. Snapshots were taken at 0 and 36 min after injection and are representative of three independent surgeries (three mice) from different imaging sessions. (inset) High magnification of two individual LNDCs. (b, left) Real-time tracking of LNDCs from panel a. LNDC tracks are highlighted (white) and final destinations marked (closed circles). (right) Vector representation of complete tracks. Green and red vectors represent LNDCs with migration paths toward or away from the PLN capsule, respectively. Data are representative of three independent surgeries (three mice) from different imaging sessions. (c) Quantitation of bulk DCs from live imaging in panel a. DC spherical index (red) and surface area (black) are displayed. ANOVA (black), $P < 0.005$; ANOVA (red), $P < 0.005$. (d) Fluorescent reconstructions of in vivo–labeled CD11c-eYFP reporter PLNs. PLNs were collected at 60 min after PBS or UV-PR8 vaccination. Data are representative of three reconstructed PLNs. B, follicles; M, medulla; MM, medullary macrophage; T, T cell cortex. (e) Quantitation of the percentage of LNDCs inside or outside of the medulla as in d ($n = 3$ PLNs). *, $P < 0.05$. Mean ± SEM.

quantified through a shift in the ratio of medulla-occupying versus total LNDCs (Fig. 1 e). Migration data were further verified through MP-IVM, through which the rapid arrival of LNDCs into the medulla could be observed (Video 2). Surprisingly, this change in both LNDC morphology and localization could not be identified after the injection of traditional adjuvants such as alum and MF59 despite extensive inflammation of the PLN, suggesting that this response may be specific toward viral antigen or endosomal TLR signaling.

Capture of viral antigen by LNDCs within interfollicular regions (IFRs)

Recent studies have identified interactions of DCs and T cells outside of the T cell area within IFRs in the stimulation of memory $CD8^+$ T cell responses (Hickman et al., 2008; León et al., 2012; Sung et al., 2012). In these studies, central memory T cells were generated after viral infection with the purpose of tracking those cells in the LN after secondary challenge. Although there is debate on the resting location within the LN, it is clear that after secondary challenge, central memory $CD8^+$ T cells are rapidly recruited to the IFRs where they undergo activation by antigen-loaded APCs. Furthermore, a study by Hickman et al. (2008) suggested a primary role for these sites in priming CD8 T cell immunity.

We hypothesized that these sites may serve as destinations for migrating LNDCs. To characterize the architectural identity of the IFRs, PLNs were in vivo labeled with antibodies against the lymphatic endothelium (a-Lyve-1) and subcapsular sinus macrophages (a-CD169) and then optically cleared for MP imaging. Projections of whole nodes after optical clearing (Ertürk et al., 2012) identified long extensions of the medulla that protruded extensively between B cell follicles and merged with the subcapsular sinus (Video 3). This observation identified two different types of IFR structure: cortical IFRs (cIFRs), which represent chemokine boundaries between the paracortex and B cell follicles, and medullary IFRs (mIFRs), which represent the most afferent connection points between the medulla and the subcapsular sinus (Fig. 2 a). Interestingly, these regions have recently been targeted by Liu et al. (2014) in vaccination attempts, resulting in greatly enhanced T cell priming. Confocal imaging of mIFRs in PBS or UV-PR8–vaccinated PLNs identified YFP^+ clusters similar to those identified in reconstruction analysis, identifying these sites as destinations for migrating LNDCs (Fig. 2 b). Histological staining confirmed that both $CD11b^{hi}$ and $CD8a^+$ LNDC

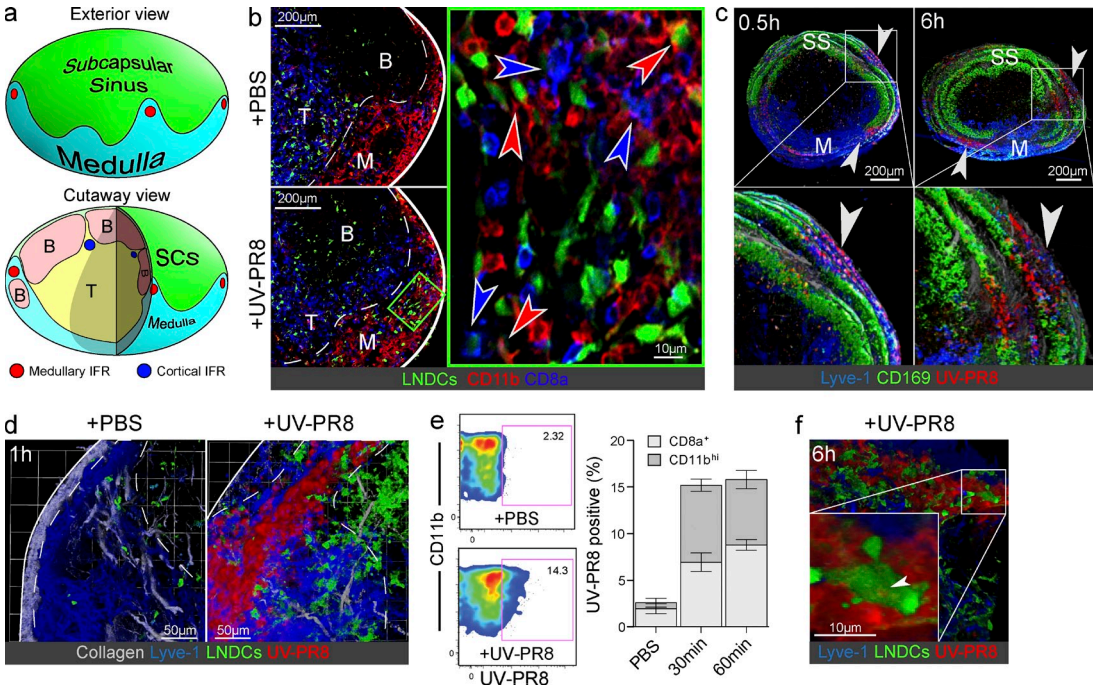

Figure 2. LNDCs infiltrate mIFRs and acquire viral antigen. (a) Schematic diagram of the architecture of a PLN. mIFRs and cIFRs are highlighted in red and blue, respectively. (b) Confocal imaging of mIFRs in CD11c-eYFP PLNs 40 min after vaccination with PBS or UV-PR8. Blue arrowheads: CD8a$^+$ DCs; red arrowheads: CD11b^{hi} DCs. Images are representative of three independent trials; three mice/trial. B, follicles; M, medulla; T, T cell cortex. (c) Reconstructions of in vivo–labeled C57BL/6 PLNs vaccinated with A633–UV-PR8 and collected at 0.5 or 6 h after injection. White arrowheads: IFRs. SS, subcapsular sinus. Images are representative of three independent experiments; two mice per time point per experiment. (d) MPM of in vivo–labeled CD11c-eYFP PLNs 60 min after PBS or A633–UV-PR8 vaccination. Dashed lines: IFRs. Images are representative of four independent experiments; two mice per experiment. (e) LNDC capture of A488–UV-PR8 by flow cytometry 60 min after injection. (left) Cells displayed are pregated to be CD11c^{hi} (n = 4 PLNs). Mean ± SEM. (f) MPM of in vivo–labeled CD11c-eYFP PLNs 6 h after A633–UV-PR8 vaccination. White arrowhead: UV-PR8 patch on the LNDC. Image is representative of four independent experiments; two mice per experiment.

populations had accumulated in mIFRs within 60 min of vaccination, suggesting a multisubset responsiveness to inactivated influenza (Fig. 2 b).

Afferent lymph flowing through the medullary sinus is constitutively filtered by sinus-lining macrophages (Gray and Cyster, 2012), and this process predicts a natural gradient of viral antigen after vaccination. Thus, it is proposed that the highest antigen concentrations would reside at the tips of these mIFRs (Video 4). To test this possibility, mice were injected s.c. with UV-PR8 labeled with Alexa Fluor 633. Fluorescent PLN reconstructions at various time points identified accumulation of viral antigen within mIFRs over 6 h after vaccination (Fig. 2 c). In contrast, lower levels of virus were retained in the subcapsular sinus and the deeper medullary compartments connecting with the efferent lymphatics. It was hypothesized that these antigen-rich regions might serve as a destination for migrating LNDCs. High-resolution imaging of IFRs bearing dense deposits of viral antigen showed large numbers of infiltrating LNDCs within 60 min of viral arrival at the node. Analysis of LNDCs by flow cytometry confirmed viral capture by both CD11b^{hi} and CD8a$^+$ LNDCs within 30 min after injection (Fig. 2 e), which was verified by MPM identifying viral patches on the surface of LNDCs at later time points (Fig. 2 f, inset).

LNDCs present viral antigen to CD4$^+$ T cells near IFRs

Previous work by Itano et al. (2003) interrogated the role of mDCs versus LNDCs in CD4$^+$ T cell stimulation. In that study, soluble peptide designed for presentation on MHC II was injected s.c., and downstream T cell responses were tracked in the draining LN. The authors observed two waves of peptide presentation, one at 6 h, which resulted in only transitory activation, and one at 18 h, which stimulated a more robust, long-term T cell response. The authors concluded that although resident DCs can activate T cells, the resident cells induce only a limited response with mDCs from the injection site required for robust immunity. To determine whether LNDCs participate in activation of viral-specific CD4$^+$ T cells within this study, CD11c-eYFP mice were adoptively transferred with labeled, ova-specific CD4$^+$ OT-II T cells 24 h before vaccination with a UV-inactive recombinant strain of PR8 (UV-PR8-OTII), which was engineered to express the OT-II epitope (Thomas et al., 2006).

As predicted, vaccination with UV-PR8-OTII stimulated activation of cognate T cells within 6 h, as indicated by CD69 up-regulation (Fig. 3 a). Although individual DC–T cell contacts could be observed as early as 6 h, extensive interaction between LNDCs and CD4$^+$ OT-II T cells was observed near IFRs by 12 h after vaccination (Fig. 3 b). Additionally, small

clusters of viral-specific T cells could be identified surrounding LNDCs in these regions. To quantitate clustering, labeled, naive OT-II T cells were transferred into CD11c-eYFP recipients, which were subsequently vaccinated with UV-PR8-OTII 12 h before LN harvesting. The LNs were serially imaged for reconstruction, and single plane images were captured from each reconstruction, representing 400 µm of vaccinated versus control LNs. Using histocytometric analysis (Gerner et al., 2012), OT-II T cells were identified within each plane, and each T cell was assessed for the number of T cell "neighbors" present in the image within one T cell diameter. The resulting measure of T cell clustering revealed significant increases in the mean number of T cell neighbors and increases in the absolute number of T cells with multiple neighbors within vaccinated versus nonvaccinated LNs (Fig. 3 c). Significantly, heat mapping the number of T cell neighbors onto the original images identified the border between the paracortex and IFRs as the most densely populated by clustered T cells (Fig. 3 d). Analysis of T cell migration at 24 h after immunization identified discreet clusters at the extremes of the paracortex, with specific colocalization of T cell clusters at the mIFR–cortical junctions (Fig. 3, e and f).

Clustering of viral-specific CD4 T cells is chemokine dependent

Previously mentioned studies describing central memory CD8 T cell responses within cIFRs have suggested the chemokine CXCR3 as a critical mediator of cellular retention in these regions. The ligands for CXCR3, CXCL9 and CXCL10, are produced by both hematopoietic and stromal cells in response to viral challenge and are critical to CD8 T cell recruitment to these sites (Sung et al., 2012; Kastenmüller et al., 2013). Additionally, Groom et al. (2012) have recently described the up-regulation of CXCR3 as an early first step in the generation of robust Th1 CD4 T cell responses. Thus, we hypothesized that the clustering of $CD4^+$ OT-II T cells with LNDCs and virus in the IFR after immunization with UV-PR8-OTII could be CXCR3 dependent. To examine whether $CD4^+$ OT-II T cells become activated and differentiate to $CXCR3^+$ T cells, LNs were harvested from immunized mice, and $CD4^+$ T cells were analyzed by flow cytometry for expression of cell surface markers of activation. Notably, an increase in CD69 expression on $CD4^+$ OT-II T cells was observed, followed by a corresponding increase in CD44 (Fig. 4 a and not depicted). By gating on newly activated $CD69^+$ cells, increases in CXCR3 expression could be identified as early as 12 h after vaccination and continued to increase over several days (Fig. 4, a and b).

As recent reporting has shown that activated DCs arriving from the periphery express CXCL10 and that direct injection of LPS/Poly I:C can induce CXCL10 expression within 12 h in the draining LN (Groom et al., 2012), it was predicted that LNDCs might express this chemokine after immunization with UV-PR8-OTII. Thus, the release of CXCL10 by activated LNDCs within the IFR could explain the extensive clustering of $CD4^+$ T cells observed within the antigen-rich IFRs. To test this possibility, CXCL9/10 reporter mice (REX3;

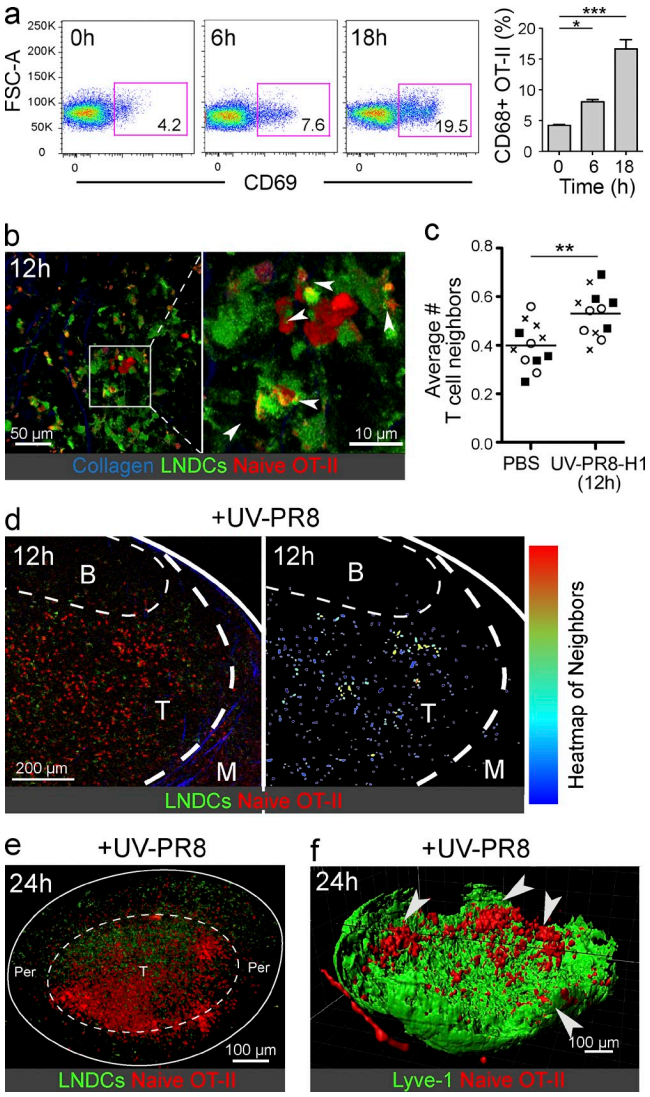

Figure 3. Cognate $CD4^+$ T cells relocate to mIFRs after vaccination. (a) C57BL/6 mice received naive OT-II T cells and were vaccinated with UV-PR8-OTII. OT-II T cell activation in PLNs was analyzed by flow cytometry ($n = 4$ mice). *, $P < 0.05$; ***, $P < 0.001$. Mean ± SEM. (b) CD11c-eYFP mice received labeled naive OT-II T cells and were vaccinated with UV-PR8-OTII. MPM of a PLN 12 h after vaccination. White arrowheads: LNDC/OT-II contacts. Images are representative of three PLNs; two independent trials. (c) OT-II neighbor analysis of PLNs as shown in b. Each symbol type represents an individual PLN, with four XY planes shown. **, $P < 0.005$. Horizontal bars indicate mean. (d) Heat map of OT-II neighbor counts as shown in c. OT-II cells were identified from images (left) and displayed with color indicative of the number of corresponding OT-II neighbors (right). B, follicles; M, medulla; T, T cell cortex. (e) CD11c-eYFP recipients received labeled naive OT-II T cells and were vaccinated with UV-PR8-OTII. Fluorescent reconstruction of a PLN 24 h after vaccination is shown. Per, PLN "periphery." Image is representative of three independent trials; two mice/trial. (f) C57BL/6 mice received OT-II T cells and were vaccinated with UV-PR8-OTII. PLNs were collected at 24 h after vaccination, optically cleared, and imaged. Data are represented with medulla isosurfacing to aid visual interpretation. White arrowheads: mIFR/T cell cluster colocalization. Image is representative of two trials; two mice/trial.

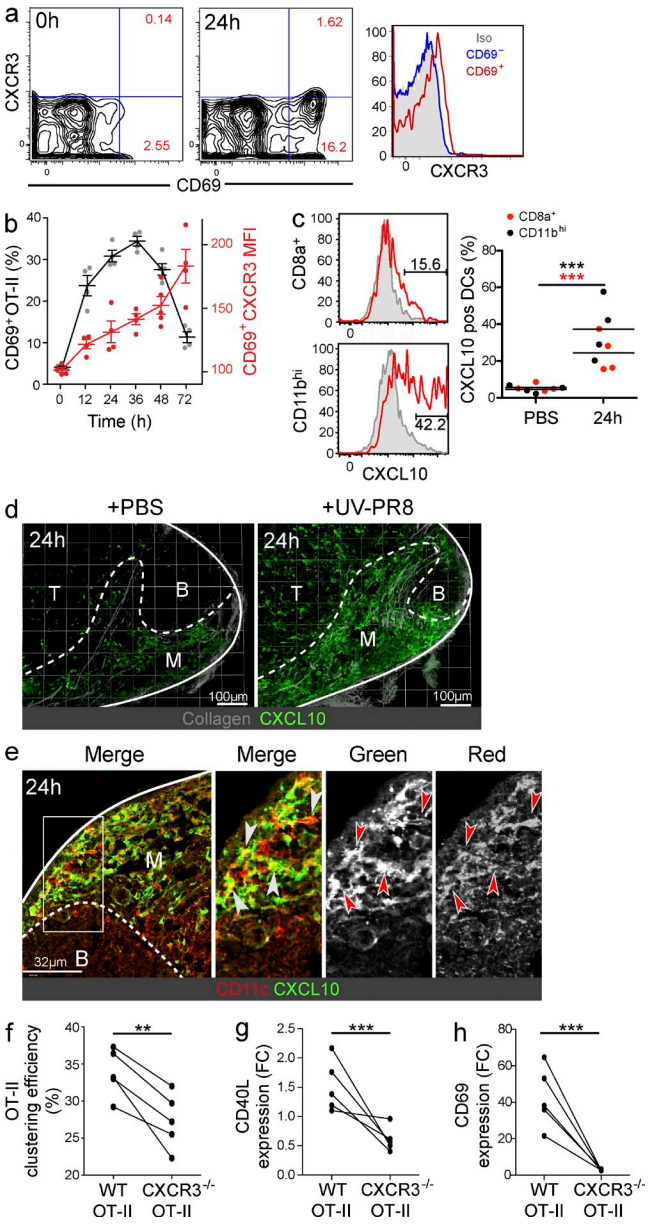

Figure 4. CXCR3-dependent clustering of viral-specific CD4⁺ T cells in mIFRs. (a) Flow cytometry of OT-II T cell activation after UV-PR8-OTII vaccination at the indicated time points ($n = 4$). (b) Expression of CD69 (black) and CXCR3 (red) by OT-II T cells at the indicated time points as in panel a. CD69⁺ OT-II cells were gated for CXCR3 expression analysis. Symbols represent individual mice. ANOVA (CD69), $P < 0.0005$; ANOVA (CXCR3), $P < 0.005$ ($n = 4$). Mean ± SEM. (c) CXCL10 expression in vaccinated REX3 mice or unvaccinated REX3 controls by flow cytometry. (left) Displayed cells gated on CD11c^{hi} cDCs, followed by CD11b^{hi} or CD8a⁺ as indicated. (right) Percentage of CXCL10-positive DCs by subset after vaccination ($n = 4$). ***, $P < 0.001$. Horizontal bars indicate mean. (d) MP imaging of REX3 PLN 24 h after UV-PR8 vaccination. Dashed line: medulla (M). B, follicles; T, T cell cortex. Images are representative of four PLNs from two independent trials. (e) Confocal imaging of REX3 PLN 24 h after UV-PR8 vaccination. Arrowheads: CXCL10-positive DCs. Images are representative of four PLNs; two independent trials. (f) C57BL/6 recipients received differentially labeled WT or CXCR3-deficient naive OT-II T cells. Recipients were vaccinated with UV-PR8-OTII, and PLNs were collected at 24 h. Quantitation of clustering efficiency of WT or CXCR3-deficient OT-II T cells is shown ($n = 5$). (g and h) Adoptive transfers were performed as in f. Recipients were vaccinated, and PLN suspensions were collected 60 h after vaccination for flow analysis. Individual T cell populations were compared with the same population in unvaccinated contralateral controls. CD40L (g) and CD69 (h) acquisition is expressed as fold change (FC) in vaccinated versus unvaccinated population controls ($n = 5$). **, $P < 0.005$; ***, $P < 0.001$.

Groom et al., 2012) were vaccinated with UV-PR8, and LNs were harvested after 24 h for analysis by flow cytometry and immunohistochemistry. Flow analysis identified the expression of CXCL10 by both CD11b^{hi} and CD8a⁺ LNDCs after vaccination (Fig. 4 c), although the CD11b^{hi} population appeared more robustly responsive. Fluorescent reconstructions of vaccinated REX3 PLNs identified high CXCL10 expression on dendritic-looking cells within mIFRs after vaccination, suggesting LNDC expression (Fig. 4 d). Confocal analysis positively identified these cells as DCs through CD11c expression and confirmed clustering of CXCL10-positive DCs within IFRs by 24 h after vaccination (Fig. 4 e). The timing of this event corresponded with both LNDC migration and formation of T cell clusters.

To confirm the importance of CXCL10 in attracting viral-specific T cells to the IFRs, mice were adoptively transferred with differentially labeled CXCR3$^{+/+}$ and CXCR3$^{-/-}$ OT-II T cells and subsequently immunized with UV-PR8-OTII virus. Characterization of the vaccinated recipients revealed a significant defect in the clustering of CXCR3$^{-/-}$ OT-II cells at 24 h after vaccination, confirming the importance of CXCR3 in T cell migration (Fig. 4 f). Additionally, flow cytometric analysis of CXCR3$^{-/-}$ OT-II T cells displayed a profound deficiency in both CD69 activation and CD40L expression (Fig. 4, g and h). These results replicate the study by Groom et al. (2012), which described early activation defects, followed by a deficient Th1 response in the absence of CXCR3. Together, these data suggest a model whereby LNDC activation of CD4⁺ T cells at early time points leads to expression of CXCR3 and contributes to the efficient localization of cognate cells into mIFRs, resulting in efficient early activation.

LNDC-dependent T cell activation

Although the activation of T cells within 6 h of vaccination suggested a role for LNDCs in early activation of CD4⁺ T cell responses to UV-PR8, it remained unclear whether skin-resident mDCs were required to establish an enduring humoral response. Using a system developed by Itano et al. (2003), the contribution of the mDC population could be effectively removed through resection of the injection site within 30 min after immunization (Kissenpfennig et al., 2005). By administering UV-PR8 intradermally in the ear and removing the ear shortly after administration, the relative contribution of mDC and LNDC populations could be evaluated in the auricular LN (ALN).

Using this approach, C57BL/6 mice were vaccinated with PBS or UV-PR8 intradermally, with half of the vaccinated group undergoing ear removal (here referred to as the van Gogh [vG] group) within 30 min after vaccine administration. Using REX3 reporter mice, expression of CXCL10 by both CD11b^{hi} and CD8a^{+} in WT or vG-vaccinated animals was assessed 24 h after injection/resection. Interestingly, although CXCL10 expression was still robust in both LNDC populations, suggesting normal responsiveness to vaccination despite a lack of mDCs in the vG group (Fig. 5 a), there was a small decrease in expression by the CD8a^{+} subset, perhaps relating to its known reliance on incoming mDCs from the periphery (Allan et al., 2006).

By transferring CFSE-labeled naive OT-II T cells into B6 recipients and using the vG vaccination system, potential deficiencies in T cell proliferation and activation could be assessed in the absence of mDCs from the injection site. Surprisingly, vG group OT-II T cells proliferated similarly to the WT group (Fig. 5 b) and could be tracked through seven divisions in 60 h. Tracking T cell activation by division status, cells could be observed acquiring both CXCR3 and CD40L as they proliferated in both the WT and vG groups (Fig. 5, c and d). Interestingly, although CD40L expression appeared identical in both groups, there was a slight delay in CXCR3 acquisition between the WT and vG group. These findings may also suggest collaboration with mDCs in reinforcing Th1 immunity development as they arrive from the periphery.

LNDC-dependent B cell memory

As LNDC and T cell activation appeared to be intact despite the absence of mDCs in the vG model, it was hypothesized that LNDCs may be sufficient to drive downstream protective humoral immunity despite the absence of mDCs. To test this hypothesis, the vG vaccination model was used in C57BL/6 mice alongside PBS-vaccinated controls. ALNs were collected at day 7 after vaccination, and germinal center staining appeared normal in both WT and vG groups, confirming effective T cell help despite the absence of mDCs (Fig. 6 a). Antibody titers collected at day 10 after vaccination showed normal increases in IgM, IgG1, and IgG2b in vG versus WT vaccination groups in comparison with unvaccinated controls, suggesting normal class switching and germinal center development (Fig. 6 b).

To test the functionality of this antibody response, vaccinated, or unvaccinated controls were challenged intratracheally with a lethal dose of live PR8 on day 21 after vaccination. Morbidity was monitored for 9 d after infection, at which point the unvaccinated control group was sacrificed as a result of excessive weight loss. Neither WT nor vG groups experienced significant weight loss over the course of infection, indicating protective immunity had been generated with or without mDC arrival from the injection site (Fig. 6, c and d). Finally, antibody titers were assessed at day 9 and compared with both unvaccinated and uninfected controls. As expected, antibody titers showed extensive class switching in both WT and vG groups, and protective IgG2b responses were identical between groups. It is worth noting that although not required for protection, IgG1 antibody titers were slightly, but insignificantly decreased

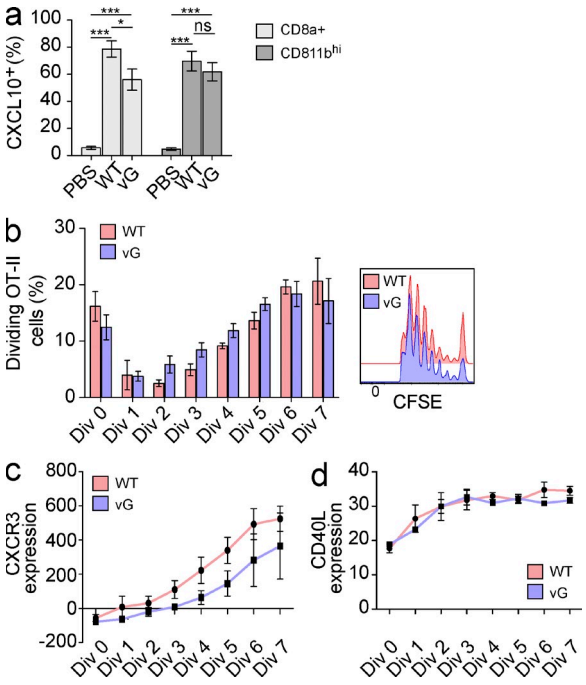

Figure 5. mDC-independent LNDC/CD4^{+} T cell activation. Ear resection in the vG model 30 min after vaccination. (a) Percentage of CD8a^{+} or CD11b^{hi} cDCs in the ALN 24 h after ear vaccination. PBS, WT, and vG groups are displayed. ANOVA (light gray), $P < 0.0001$; ANOVA (dark gray), $P < 0.0001$ ($n = 4$). *, $P < 0.05$; ***, $P < 0.001$. (b) CFSE-labeled OT-II T cells were transferred into C57BL/6 recipients. Recipients were vaccinated in the ear and separated into WT and vG groups. ALNs were isolated at 60 h after injection and analyzed by flow cytometry. (left) Percentage of OT-II T cells by division number as assessed by CFSE dilution. ANOVA, $P > 0.1$. (right) Representative plot of CFSE dilution in WT and vG groups ($n = 4$ mice/group). (c and d) Adoptive transfers were established as in c. OT-II T cell expression (MFI) of CXCR3 (c) and CD40L (d) was assessed by T cell division to track acquisition over time. (c) Two-way ANOVA, $P < 0.0001$ overall, $P < 0.05$ between groups. (d) Two-way ANOVA, $P < 0.0001$ overall, $P > 0.1$ between groups ($n = 4$ mice/group). Mean ± SEM.

in the vG group, providing additional evidence for LNDC/mDC collaboration in a vaccination setting. Altogether, these data demonstrate that LNDCs are capable of stimulating CD4^{+} Th1-dependent protective humoral responses to influenza vaccination.

DISCUSSION

An earlier study identifying capture of lymph-borne inactive influenza virus by LNDCs raised the question of the relative importance of this population in overall humoral immunity (Gonzalez et al., 2010). To gain a broader understanding of LNDCs in response to vaccination with inactive influenza, a whole-node imaging approach was developed, and mice bearing a fluorescent reporter for DCs (CD11c^{+}) were vaccinated with UV-PR8. After s.c. vaccination, viral antigen was observed within the draining LN within minutes, as expected. Surprisingly, however, the virus accumulated over the first 6 h within specialized sites identified as mIFRs.

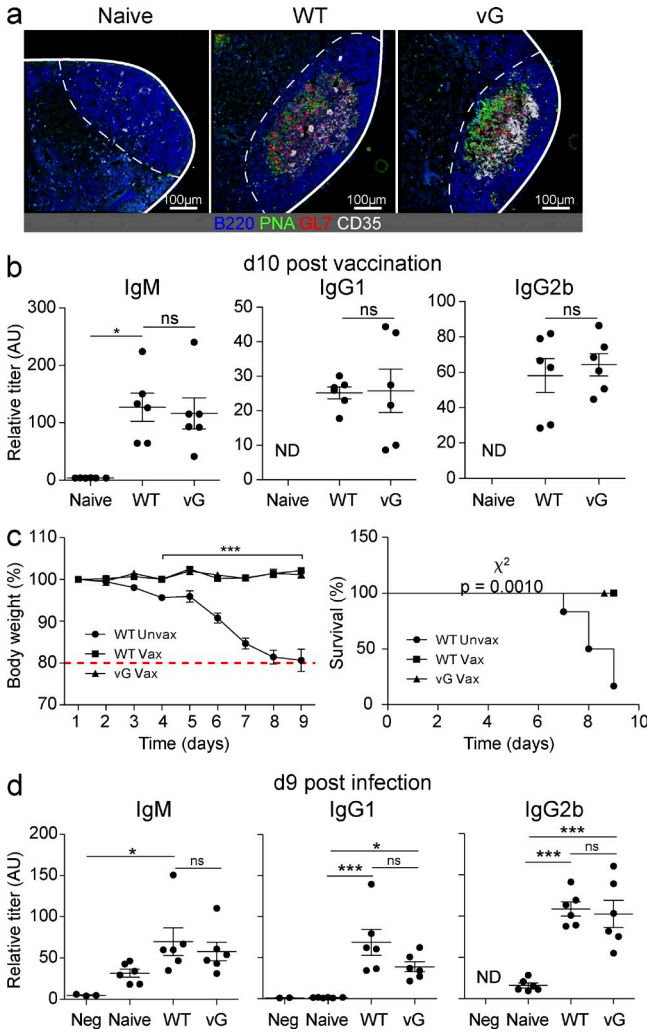

Figure 6. mDC-independent protection from influenza. (a) Confocal imaging of ALN follicles at day 10 after UV-PR8 vaccination in WT and vG mice. Dashed line: B cell follicle. Images are representative of two independent trials; five mice/group. (b) ELISA analysis of PR8-specific serum antibodies at day 10 after UV-PR8 vaccination. Relative titers of PR8-specific IgM, IgG1, and IgG2b are shown. Symbols represent individual animals. (c) Unvaccinated or vaccinated WT or vG groups were challenged with LD80 PR8 21 d after vaccination. Morbidity (left) and mortality (right) are displayed as percentage of body weight or percent survival, respectively. Red dashed line: morbidity/euthanasia experimental cutoff. Six mice/group. (d) ELISA analysis of PR8-specific serum antibodies at day 9 after PR8 challenge as in c, compared with naive C57BL/6 littermates. Relative titers of PR8-specific IgM, IgG1, and IgG2b are shown. Symbols represent individual animals. *, $P < 0.05$; ***, $P < 0.001$. Mean ± SEM.

Using fluorescent reconstructions of full PLNs isolated at early time points after vaccination, we observed a major repositioning of LNDCs from the T cell cortex to the mIFR where they acquired viral antigen and became activated. This was unexpected because LNDCs are reported to be relatively sessile at steady-state. The capture of virus by the resident DC was biologically relevant because they became positive for the chemokine CXCL10 and formed clusters with viral-specific $CD4^+$ T cells that became activated based on expression of CD69, CD44, and CXCR3. Thus, three lines of evidence are presented that support a role for LNDCs in promoting a humoral response to inactive PR8 independent of mDCs: (1) activation of viral-specific $CD4^+$ T cells before expected arrival of skin mDCs, (2) activation of viral-specific $CD4^+$ T cells within PLNs in the absence of mDCs, and (3) a normal humoral memory response despite surgical removal of the injection site within 30 min of vaccination. Notably, although these findings clearly demonstrate sufficiency of the resident DC population in establishing humoral immunity, they do not address the requirement of mDCs under conditions where lymph-borne antigen is not readily available.

Although several groups have previously described resident DC populations in skin-draining LNs (Lindquist et al., 2004), few have directly assessed their potential in presenting antigen acquired directly from the lymph. In one study, Itano et al. (2003) describe a two-step process of antigen presentation where resident DCs in the LN were capable of acquisition and presentation of soluble peptides, but skin-resident mDCs were required for effective immunity. In another study, Allenspach et al. (2008) found that in the case of soluble peptide administered with CFA, resident DCs were similarly deficient in T cell presentation. Our findings are not inconsistent with these results, as the robust activation/migration of resident DCs cannot be identified after traditional adjuvant administration (alum or MF59). The profound differences in these responses also raise interesting questions about a potential gap between traditional vaccination approaches and natural response to viral antigen. As medullary macrophages rapidly degrade protein antigen as a part of normal lymphatic filtration, it is important to understand how to maximize antigen exposure to efficient antigen presenters, especially when antigen concentration is highest immediately after vaccination. Data from this study suggest that LNDCs are capable of effectively using antigen when appropriately stimulated and could represent an efficient target for vaccination approaches.

An unexpected observation was the rapid kinetics of LNDC repositioning from the paracortical region to the mIFR in response to localization of viral antigen. Although large deposits of LNDCs were observed in viral-loaded IFRs within hours of vaccination, individual LNDC morphological changes could be observed within 12 min of vaccination. The highly directional migration pattern of LNDCs to the sites of viral accumulation suggests a response to chemotactic mediators released from a prestored source after innate sensing of viral antigen, although this source remains yet unclear.

A recent study has identified CXCR3 and its ligands CXCL9 and CXCL10 as required for migration of CD8 memory T cells into IFRs, where they make contact with both antigen and APCs (Sung et al., 2012). Although the distinction between mIFRs and cIFRs was not made in these studies, it is clear that this chemoattractant is important in various conditions of immune response. In our study, formation of clusters of viral-specific $CD4^+$ T cells with LNDCs was significantly reduced in $CXCR3^{-/-}$ OT-II T cells. Because

CXCL10 expression is not restricted to LNDCs, this pathway might provide an efficient mechanism for collaboration between LNDCs and incoming mDCs, whereby early activation of naive CD4 T cells, and concomitant expression of CXCR3, allows activated T cells to more easily find mDCs from the injection site, which also express CXCL10. Additionally, it is possible that mDCs might be able to locate hot spots of immune activation within the LN through their own expression of CXCR3.

In summary, using novel whole-node imaging approaches, we observed a multistep system of immune activation whereby viral antigen, LNDCs, and cognate naive $CD4^+$ T cells rapidly assemble in highly organized environments within the draining LNs known to be relevant to vaccine design (Liu et al., 2014). In addition to identifying an unexpected repositioning of LNDCs to specialized sites within the draining LN, these findings clarify the importance of CXCR3 in establishing immunostimulatory microenvironments in three dimensions and establish LNDCs as biologically relevant cell populations, sufficient to drive humoral memory response to an influenza vaccine in the absence of mDCs.

MATERIALS AND METHODS

Animals. Mice used in this study were bred and housed in standard conditions and used between 6 and 12 wk of age. All experimental protocols were approved through Harvard University's Institutional Animal Care and Use Committee.

In vivo labeling. In vivo labeling of the PLN subcapsular sinus and medulla was achieved through injection of Alexa Fluor–conjugated (A488, A568, A633) antibody targeting stromal (a–LYVE-1) or macrophage populations (a-CD169, a-SIGNR1, a-F4/80) s.c. in the footpad 4 h before PLN imaging or tissue harvest.

PLN live imaging. PLN live imaging was performed through surgical exposure of the PLN in anesthetized mice and MPM. Temperature was monitored using a digital thermometer embedded in the imaging chamber created around the PLN and controlled using a closed-circuit water circulation system (Lindquist et al., 2004; Gonzalez et al., 2010).

Three-dimensional reconstruction. Collected organs were fixed in 4% PFA, embedded in OCT, and serially cryosectioned (50 µm). PLN sections were serially imaged by MPM and assembled using Imaris software (Bitplane) to obtain three-dimensional reconstructions. Final analysis was performed using Volocity image analysis software (PerkinElmer).

Whole-organ imaging. LNs were dissected and fixed overnight in 4% paraformaldehyde. The sample was then incubated in increasing concentrations of tetrahydrofuran followed by dichloromethane. Finally, the PLN was immersed in BABB (benzyl alcohol/benzyl benzoate, mix 1:2) for final clearing and imaging (Lindquist et al., 2004; Ertürk et al., 2012).

Viral propagation/labeling. Influenza virus was grown in live chicken eggs, purified over sucrose gradients (Szretter et al., 2006; Gonzalez et al., 2010), and labeled using standard Alexa Fluor–labeling protocol (Invitrogen). 10–20-µl s.c. injections were given in the footpad at 10^6 PFU.

T cell isolation. LNs of OT-II mice were processed using Liberase DH (Sigma-Aldrich) digestion, and T cells were isolated through MACS negative selection (CD11c, CD11b, NK1.1, B220, GR-1, CD69, CD8). T cells were labeled in 10 µm CMTMR for imaging or 5 µM CFSE for imaging and flow cytometric identification. 1 or 5×10^6 cells were adoptively transferred into naive recipients for flow cytometric or imaging experiments, respectively.

Three-dimensional image analysis. Images were processed and analyzed using Volocity imaging software. Histocytometric analysis of reconstructions was performed with CellProfiler (Carpenter et al., 2006; Grigorova et al., 2010), and CellProfiler Analyst (Hickman et al., 2008; Jones et al., 2008; León et al., 2012). Analysis of reconstructions was performed with individual XY imaging planes, which were representative of at least 400 µm of reconstructed LNs.

T cell clustering. $CXCR3^{-/-}$ and WT OT-II cells were isolated as above, differentially labeled, and adoptively transferred into C57BL/6 recipients. PLNs were collected, processed, and serially imaged 24 h after vaccination with UV-PR8-OTII. T cell clusters were identified using a blinded approach, and the percentage of each population within these clusters was measured.

Ear resections. Ear removal was performed 30 min after injection of 10 µl PBS or UV-PR8 s.c. between the ear dermal layers. ELISA analysis of serum was performed through immobilization of UV-PR8 on the plate, addition of serum, and probing for specific binding of IgM, IgG1, or IgG2b.

Statistics. All statistics/graphical representations of collected data were assembled through Prism (GraphPad Software). Mean and SEM are displayed where applicable. Results from Student's *t* tests or Tukey's post tests are indicated by asterisks in the figures (*, $P < 0.05$; **, $P < 0.005$; ***, $P < 0.001$). One- or two-way ANOVA testing is indicated in the legends.

Online supplemental material. Video 1 shows LNDC migration in response to influenza vaccination. Video 2 shows that LNDCs infiltrate the medulla after UV-PR8 vaccination. Video 3 shows reconstruction of a PLN. Video 4 shows lymph flow through the PLN. Online supplemental material is available at http://www.jem.org/cgi/content/full/jem.20132327/DC1.

We thank J. Campbell for providing CCR7-deficient mice, N. Anandasabapathy and S. Jones for critical discussion and review of this manuscript, and H. Leung, E. Carroll, S. Lavoie, and M. Ma for technical support.

This work was supported by the National Institutes of Health (NIH)–National Institute of Allergy and Infectious Diseases (grants 1 P01 AI078897, R37 AI054636, and R01 AI039246 to M.C. Carroll; R01CA069212 to A.D. Luster; RO1 DK074500 and PO1 AI045757 to S.J. Turley; and AI107625 to P.G. Thomas), NIH T32 Training Grant in Transplantation (T32 AI007498 to M.C. Woodruff), the American Lung Association (grant RT-224269-N to C.N. Herndon), and the National Health and Medical Research Council, Australia (fellowship 516791 to J.R. Groom).

The authors declare no competing financial interests.

Author contributions: M.C. Woodruff, B.A. Heesters, and C.N. Herndon performed all experiments and analysis described in the text. P.G. Thomas, J.R. Groom, and A.D. Luster developed critical reagents for the completion of the study. M.C. Woodruff, S.J. Turley, and M.C. Carroll designed this study and developed the manuscript for publication.

Submitted: 6 November 2013
Accepted: 19 June 2014

REFERENCES

Acton, S.E., J.L. Astarita, D. Malhotra, V. Lukacs-Kornek, B. Franz, P.R. Hess, Z. Jakus, M. Kuligowski, A.L. Fletcher, K.G. Elpek, et al. 2012. Podoplanin-rich stromal networks induce dendritic cell motility via activation of the C-type lectin receptor CLEC-2. *Immunity*. 37:276–289. http://dx.doi.org/10.1016/j.immuni.2012.05.022

Allan, R.S., J. Waithman, S. Bedoui, C.M. Jones, J.A. Villadangos, Y. Zhan, A.M. Lew, K. Shortman, W.R. Heath, and F.R. Carbone. 2006. Migratory dendritic cells transfer antigen to a lymph node-resident dendritic cell population for efficient CTL priming. *Immunity*. 25:153–162. http://dx.doi.org/10.1016/j.immuni.2006.04.017

Allenspach, E.J., M.P. Lemos, P.M. Porrett, L.A. Turka, and T.M. Laufer. 2008. Migratory and lymphoid-resident dendritic cells cooperate to efficiently prime naive CD4 T cells. *Immunity*. 29:795–806. http://dx.doi.org/10.1016/j.immuni.2008.08.013

Alvarez, D., E.H. Vollmann, and U.H. von Andrian. 2008. Mechanisms and consequences of dendritic cell migration. *Immunity*. 29:325–342. http://dx.doi.org/10.1016/j.immuni.2008.08.006

Arnason, J., and D. Avigan. 2012. Evolution of cellular immunotherapy: from allogeneic transplant to dendritic cell vaccination as treatment for multiple myeloma. *Immunotherapy*. 4:1043–1051. http://dx.doi.org/10.2217/imt.12.118

Austyn, J.M. 1996. New insights into the mobilization and phagocytic activity of dendritic cells. *J. Exp. Med.* 183:1287–1292. http://dx.doi.org/10.1084/jem.183.4.1287

Braun, A., T. Worbs, G.L. Moschovakis, S. Halle, K. Hoffmann, J. Bölter, A. Münk, and R. Förster. 2011. Afferent lymph-derived T cells and DCs use different chemokine receptor CCR7-dependent routes for entry into the lymph node and intranodal migration. *Nat. Immunol.* 12:879–887. http://dx.doi.org/10.1038/ni.2085

Carpenter, A.E., T.R. Jones, M.R. Lamprecht, C. Clarke, I.H. Kang, O. Friman, D.A. Guertin, J.H. Chang, R.A. Lindquist, J. Moffat, et al. 2006. CellProfiler: image analysis software for identifying and quantifying cell phenotypes. *Genome Biol.* 7:R100. http://dx.doi.org/10.1186/gb-2006-7-10-r100

Carrasco, Y.R., and F.D. Batista. 2007. B cells acquire particulate antigen in a macrophage-rich area at the boundary between the follicle and the subcapsular sinus of the lymph node. *Immunity*. 27:160–171. http://dx.doi.org/10.1016/j.immuni.2007.06.007

Ertürk, A., C.P. Mauch, F. Hellal, F. Förstner, T. Keck, K. Becker, N. Jährling, H. Steffens, M. Richter, M. Hübener, et al. 2012. Three-dimensional imaging of the unsectioned adult spinal cord to assess axon regeneration and glial responses after injury. *Nat. Med.* 18:166–171. http://dx.doi.org/10.1038/nm.2600

Gerner, M.Y., W. Kastenmuller, I. Ifrim, J. Kabat, and R.N. Germain. 2012. Histo-cytometry: a method for highly multiplex quantitative tissue imaging analysis applied to dendritic cell subset microanatomy in lymph nodes. *Immunity*. 37:364–376. http://dx.doi.org/10.1016/j.immuni.2012.07.011

Gonzalez, S.F., V. Lukacs-Kornek, M.P. Kuligowski, L.A. Pitcher, S.E. Degn, Y.-A. Kim, M.J. Cloninger, L. Martinez-Pomares, S. Gordon, S.J. Turley, and M.C. Carroll. 2010. Capture of influenza by medullary dendritic cells via SIGN-R1 is essential for humoral immunity in draining lymph nodes. *Nat. Immunol.* 11:427–434. http://dx.doi.org/10.1038/ni.1856

Gray, E.E., and J.G. Cyster. 2012. Lymph node macrophages. *J. Innate Immun.* 4:424–436. http://dx.doi.org/10.1159/000337007

Grigorova, I.L., M. Panteleev, and J.G. Cyster. 2010. Lymph node cortical sinus organization and relationship to lymphocyte egress dynamics and antigen exposure. *Proc. Natl. Acad. Sci. USA*. 107:20447–20452. http://dx.doi.org/10.1073/pnas.1009968107

Groom, J.R., J. Richmond, T.T. Murooka, E.W. Sorensen, J.H. Sung, K. Bankert, U.H. von Andrian, J.J. Moon, T.R. Mempel, and A.D. Luster. 2012. CXCR3 chemokine receptor-ligand interactions in the lymph node optimize $CD4^+$ T helper 1 cell differentiation. *Immunity*. 37:1091–1103. http://dx.doi.org/10.1016/j.immuni.2012.08.016

Hickman, H.D., K. Takeda, C.N. Skon, F.R. Murray, S.E. Hensley, J. Loomis, G.N. Barber, J.R. Bennink, and J.W. Yewdell. 2008. Direct priming of antiviral $CD8^+$ T cells in the peripheral interfollicular region of lymph nodes. *Nat. Immunol.* 9:155–165. http://dx.doi.org/10.1038/ni1557

Hill, M., M. Segovia, and M.C. Cuturi. 2011. What is the role of antigen-processing mechanisms in autologous tolerogenic dendritic cell therapy in organ transplantation? *Immunotherapy*. 3:12–14. http://dx.doi.org/10.2217/imt.11.40

Itano, A.A., S.J. McSorley, R.L. Reinhardt, B.D. Ehst, E. Ingulli, A.Y. Rudensky, and M.K. Jenkins. 2003. Distinct dendritic cell populations sequentially present antigen to CD4 T cells and stimulate different aspects of cell-mediated immunity. *Immunity*. 19:47–57. http://dx.doi.org/10.1016/S1074-7613(03)00175-4

Jones, T.R., I.H. Kang, D.B. Wheeler, R.A. Lindquist, A. Papallo, D.M. Sabatini, P. Golland, and A.E. Carpenter. 2008. CellProfiler Analyst: data exploration and analysis software for complex image-based screens. *BMC Bioinformatics*. 9:482. http://dx.doi.org/10.1186/1471-2105-9-482

Junt, T., E.A. Moseman, M. Iannacone, S. Massberg, P.A. Lang, M. Boes, K. Fink, S.E. Henrickson, D.M. Shayakhmetov, N.C. Di Paolo, et al. 2007. Subcapsular sinus macrophages in lymph nodes clear lymph-borne viruses and present them to antiviral B cells. *Nature*. 450:110–114. http://dx.doi.org/10.1038/nature06287

Kastenmüller, W., M. Brandes, Z. Wang, J. Herz, J.G. Egen, and R.N. Germain. 2013. Peripheral prepositioning and local CXCL9 chemokine-mediated guidance orchestrate rapid memory $CD8^+$ T cell responses in the lymph node. *Immunity*. 38:502–513. http://dx.doi.org/10.1016/j.immuni.2012.11.012

Kissenpfennig, A., S. Henri, B. Dubois, C. Laplace-Builhé, P. Perrin, N. Romani, C.H. Tripp, P. Douillard, L. Leserman, D. Kaiserlian, et al. 2005. Dynamics and function of Langerhans cells in vivo: dermal dendritic cells colonize lymph node areas distinct from slower migrating Langerhans cells. *Immunity*. 22:643–654. http://dx.doi.org/10.1016/j.immuni.2005.04.004

Lämmermann, T., B.L. Bader, S.J. Monkley, T. Worbs, R. Wedlich-Söldner, K. Hirsch, M. Keller, R. Förster, D.R. Critchley, R. Fässler, and M. Sixt. 2008. Rapid leukocyte migration by integrin-independent flowing and squeezing. *Nature*. 453:51–55. http://dx.doi.org/10.1038/nature06887

Larsen, C.P., R.M. Steinman, M. Witmer-Pack, D.F. Hankins, P.J. Morris, and J.M. Austyn. 1990. Migration and maturation of Langerhans cells in skin transplants and explants. *J. Exp. Med.* 172:1483–1493. http://dx.doi.org/10.1084/jem.172.5.1483

León, B., A. Ballesteros-Tato, J.L. Browning, R. Dunn, T.D. Randall, and F.E. Lund. 2012. Regulation of T_H2 development by $CXCR5^+$ dendritic cells and lymphotoxin-expressing B cells. *Nat. Immunol.* 13:681–690. http://dx.doi.org/10.1038/ni.2309

Lindquist, R.L., G. Shakhar, D. Dudziak, H. Wardemann, T. Eisenreich, M.L. Dustin, and M.C. Nussenzweig. 2004. Visualizing dendritic cell networks in vivo. *Nat. Immunol.* 5:1243–1250. http://dx.doi.org/10.1038/ni1139

Liu, H., K.D. Moynihan, Y. Zheng, G.L. Szeto, A.V. Li, B. Huang, D.S. Van Egeren, C. Park, and D.J. Irvine. 2014. Structure-based programming of lymph-node targeting in molecular vaccines. *Nature*. 507:519–522. http://dx.doi.org/10.1038/nature12978

Llanos, C., L.J. Carreño, and A.M. Kalergis. 2011. Contribution of dendritic cell/T cell interactions to triggering and maintaining autoimmunity. *Biol. Res.* 44:53–61. http://dx.doi.org/10.4067/S0716-97602011000100007

Moodycliffe, A.M., I. Kimber, and M. Norval. 1994. Role of tumour necrosis factor-alpha in ultraviolet B light-induced dendritic cell migration and suppression of contact hypersensitivity. *Immunology*. 81:79–84.

Phan, T.G., I. Grigorova, T. Okada, and J.G. Cyster. 2007. Subcapsular encounter and complement-dependent transport of immune complexes by lymph node B cells. *Nat. Immunol.* 8:992–1000. http://dx.doi.org/10.1038/ni1494

Poudrier, J., J. Chagnon-Choquet, and M. Roger. 2012. Influence of dendritic cells on B-cell responses during HIV infection. *Clin. Dev. Immunol.* 2012:592187. http://dx.doi.org/10.1155/2012/592187

Qi, H., J.G. Egen, A.Y.C. Huang, and R.N. Germain. 2006. Extrafollicular activation of lymph node B cells by antigen-bearing dendritic cells. *Science*. 312:1672–1676. http://dx.doi.org/10.1126/science.1125703

Randolph, G.J., V. Angeli, and M.A. Swartz. 2005. Dendritic-cell trafficking to lymph nodes through lymphatic vessels. *Nat. Rev. Immunol.* 5:617–628. http://dx.doi.org/10.1038/nri1670

Rescigno, M., C. Winzler, D. Delia, C. Mutini, M. Lutz, and P. Ricciardi-Castagnoli. 1997. Dendritic cell maturation is required for initiation of the immune response. *J. Leukoc. Biol.* 61:415–421.

Roozendaal, R., T.R. Mempel, L.A. Pitcher, S.F. Gonzalez, A. Verschoor, R.E. Mebius, U.H. von Andrian, and M.C. Carroll. 2009. Conduits mediate transport of low-molecular-weight antigen to lymph node follicles. *Immunity*. 30:264–276. http://dx.doi.org/10.1016/j.immuni.2008.12.014

Steinman, R.M. 1991. The dendritic cell system and its role in immunogenicity. *Annu. Rev. Immunol.* 9:271–296. http://dx.doi.org/10.1146/annurev.iy.09.040191.001415

Steinman, R.M., M. Pack, and K. Inaba. 1997. Dendritic cells in the T-cell areas of lymphoid organs. *Immunol. Rev.* 156:25–37. http://dx.doi.org/10.1111/j.1600-065X.1997.tb00956.x

Sung, J.H., H. Zhang, E.A. Moseman, D. Alvarez, M. Iannacone, S.E. Henrickson, J.C. de la Torre, J.R. Groom, A.D. Luster, and U.H. von Andrian. 2012. Chemokine guidance of central memory T cells is critical for antiviral recall responses in lymph nodes. *Cell*. 150:1249–1263. http://dx.doi.org/10.1016/j.cell.2012.08.015

Szakal, A.K., K.L. Holmes, and J.G. Tew. 1983. Transport of immune complexes from the subcapsular sinus to lymph node follicles on the surface of nonphagocytic cells, including cells with dendritic morphology. *J. Immunol.* 131:1714–1727.

Szretter, K.J., A.L. Balish, and J.M. Katz. 2006. Influenza: propagation, quantification, and storage. *Curr. Protoc. Microbiol.* Chapter 15:Unit 15G.1.

Tal, O., H.Y. Lim, I. Gurevich, I. Milo, Z. Shipony, L.G. Ng, V. Angeli, and G. Shakhar. 2011. DC mobilization from the skin requires docking to immobilized CCL21 on lymphatic endothelium and intralymphatic crawling. *J. Exp. Med.* 208:2141–2153. http://dx.doi.org/10.1084/jem.20102392

Thomas, P.G., S.A. Brown, W. Yue, J. So, R.J. Webby, and P.C. Doherty. 2006. An unexpected antibody response to an engineered influenza virus modifies CD8+ T cell responses. *Proc. Natl. Acad. Sci. USA.* 103:2764–2769. http://dx.doi.org/10.1073/pnas.0511185103

Yen, J.-H., T. Khayrullina, and D. Ganea. 2008. PGE2-induced metalloproteinase-9 is essential for dendritic cell migration. *Blood.* 111:260–270. http://dx.doi.org/10.1182/blood-2007-05-090613